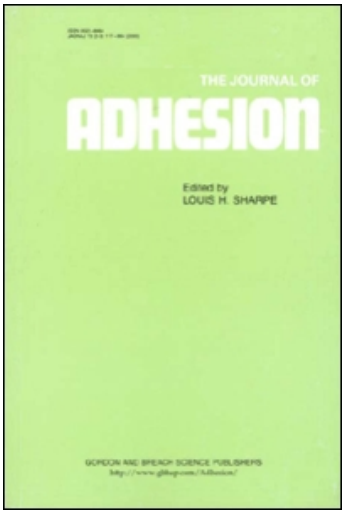

The Journal of Adhesion
Publication details, including instructions for authors and subscription information:
http://www.informaworld.com/smpp/title~content=t713453635

Stress Analysis and Failure Properties of Carbon-Fibre-Reinforced-Plastic/Steel Double-Lap Joints

R. D. Adams[a]; R. W. Atkins[b]; J. A. Harris[c]; A. J. Kinloch[d]
[a] Dept. of Mechanical Engineering, University of Bristol, Bristol [b] U. K. Ministry of Defence, Waltham Abbey, Essex [c] Malaysian Rubber Producers' Research Association, Brickendonbury, Hertford [d] Ministry of Defence, Waltham Abbey, now Dept. of Mechanical Engineering, Imperial College, London, England

To cite this Article Adams, R. D. , Atkins, R. W. , Harris, J. A. and Kinloch, A. J.(1986) 'Stress Analysis and Failure Properties of Carbon-Fibre-Reinforced-Plastic/Steel Double-Lap Joints', The Journal of Adhesion, 20: 1, 29 — 53
To link to this Article: DOI: 10.1080/00218468608073238
URL: http://dx.doi.org/10.1080/00218468608073238

J. Adhesion, 1986, Vol. 20, pp. 29–53
0021-8464/86/2001–0029 $18.50/0

Printed in the United Kingdom

Stress Analysis and Failure Properties of Carbon-Fibre-Reinforced-Plastic/Steel Double-Lap Joints

R. D. ADAMS,† R. W. ATKINS,‡ J. A. HARRIS§ and A. J. KINLOCH‖

† *Dept. of Mechanical Engineering, University of Bristol, Bristol BS8 1TR;*
‡ *U.K. Ministry of Defence, Waltham Abbey, Essex EN9 1AX;* § *Malaysian Rubber Producers' Research Association, Brickendonbury, Hertford SG13 8NL;*
‖ *Ministry of Defence, Waltham Abbey, now Dept. of Mechanical Engineering, Imperial College, London SW7 2BX, England.*

(Received 30 November 1985; in final form 14 January 1986)

The present paper considers the strength of CFRP/steel double-lap joints loaded in tension. A detailed stress analysis has been conducted of the shear and transverse tensile stresses in the joint, using an elastic-plastic model for the rubber-modified epoxy adhesive. The results of this analysis have been combined with the measured properties of the materials forming the joint in order to predict quantitatively the failure strengths of the various joint designs studied. There was good agreement between the theoretically predicted and experimentally measured strengths. These studies have led to a highly efficient design being developed.

KEY WORDS Carbon-fibre-reinforced epoxy; double lap joints; epoxy adhesive; failure properties; joint design; stress analysis.

INTRODUCTION

For joining carbon-fibre-reinforced-plastic (CFRP) to other materials, such as high-tensile steel, the use of structural adhesive bonding is a most attractive method for many reasons. For example, compared to other techniques, such as bolting, riveting, etc., it

offers improved fatigue resistance, the ability to join thin sheets of material efficiently, and greater design flexibility. However, to utilise these advantages fully, the engineer needs to understand the various design parameters which influence the strength of structural adhesive joints.

In the present paper, the strengths of CFRP/steel double-lap joints loaded in tension are considered. The aims of the work were:

i) to analyse the stress distributions in the joints,

ii) to combine these data with suitable material parameters to predict the theoretical failure strengths.

iii) to examine the agreement between theory and experiment, and

iv) to use these studies to optimise the design of the joint in order to attain a significantly increased failure strength.

THEORETICAL

Introduction

In a double-lap joint loaded in tension (Figure 1) the applied tensile load causes a distribution of both shear and tensile stresses in the adhesive layer and in the adherends.

The shear deformation in the adhesive is concentrated at the ends of the overlap (length L) as a consequence of the well-known shear-lag effect caused by differential straining in the adherends, leading to a concentration of shear stress at the ends of the overlap. This was first analysed by Volkersen[1] and more recently has been considered in detail by Hart-Smith.[2]

Also, as indicated in Figure 1, internal bending moments, M, are established in the joint, which Volkersen[3] accounted for in his later work, so that direct stresses arise, acting normal to the adhesive layer. The maximum values of these direct stresses occur in the adhesive and the inner CFRP adherend at the end of the overlap where the outer steel adherends terminate. These so-called "peel stresses" in this region have a significant influence on the failure of the joint. This arises for two reasons: firstly, the strain capability of structural adhesives is very limited in tension, as compared with

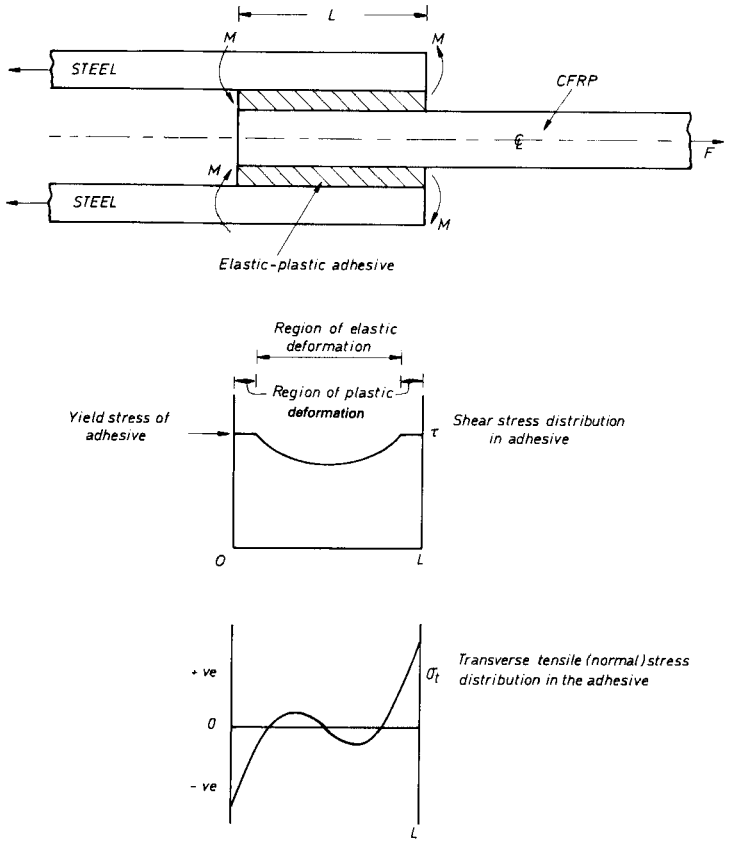

FIGURE 1 Schematic of double-lap joint loaded in tension and stress distribution in adhesive layer.

shear[4] and, secondly, the transverse tensile strength of fibrous composites is much lower than the strength parallel to the fibres.[5]

In order to predict the theoretical failure strength of a joint, it is necessary to combine the results from an analysis of the shear and tensile stresses in the joint with suitable failure criteria. Indeed, many analytical and numerical solutions for the state of stress in adhesive joints have been published, which, whilst giving a qualitative assessment of the effects of various parameters, do not enable joint strengths to be predicted. It has been recently stated that

"although numerous researchers have investigated the state of stress within a bonded composite joint, few have made an attempt to predict actual failure loads. Also, most of these prediction techniques assume a failure of the adhesive and do not address the problem of interlaminar composite adherend failure."[6] This situation has arisen for several reasons. Firstly, a complete analysis of the various components of stress is required, including variations through the thickness of both the adhesive and the adherends. Secondly, the non-linear properties of the adhesive must be included if realistic materials are to be modelled. Thirdly, in practice the joint strength may be significantly influenced by the local geometry in the critical regions of the joint, such as at the ends of the overlap. So it may be necessary, for example, to account for the existence of a fillet of adhesive at the ends of the overlap.

The present theoretical studies draw upon both established analytical and original finite element analyses to describe the shear and tensile stress distributions in the CFRP/steel joints, taking into account the above comments. Such analyses are then combined with appropriate physical properties of the materials forming the joint in order to predict the failure load of the joint as a function of various parameters.

Joint design

Since for the double lap joint, like many adhesive joint configurations, the maximum stresses occur in the regions at the edges of the adhesive layer, ways of improving joint strength by locally modifying the geometry of the joint in these regions may be possible. The existence of an adhesive fillet at the edge of the adhesive layer has been shown, using finite element techniques, to reduce the maximum stresses in the adhesive.[7] Also, it has been shown by closed form analysis of the lap joint that, by tapering the adherends to an almost 'razor edge', the peak stresses in the adhesive may be reduced. These two methods of improving joint strength have been considered in a series of joint designs illustrated in Figure 2. The dimensions of the basic design were determined from the results of the shear-lag analysis given later. Modifications to the basic design fall into three categories: in designs 2 and 3 the outer steel adherends are tapered with a 10:1 gradient and the edge of the

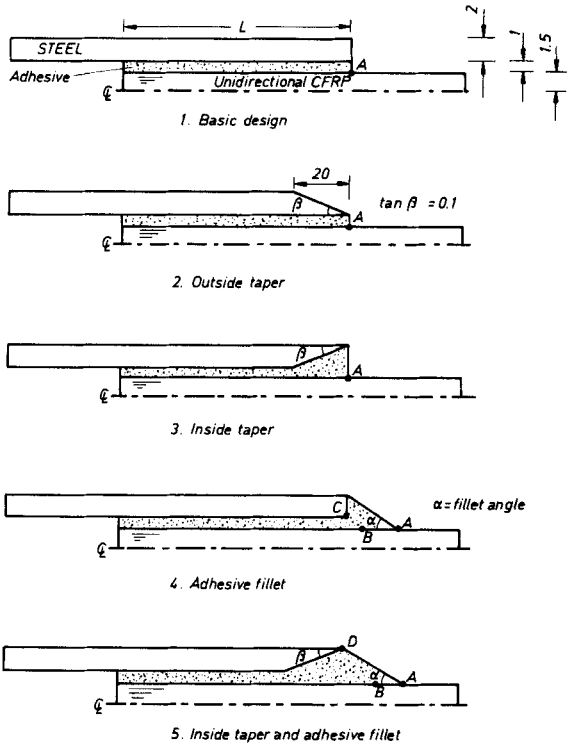

FIGURE 2 Designs of double-lap joints considered (dimensions in mm).

adhesive layer is square; in design 4 the adherends are unmodified, but adhesive fillets, whose size is defined by the angle 'α', are included; finally, in design 5, both the tapered adherends and adhesive fillets are included together.

Stress analysis

Shear stresses The distribution of shear stresses and strains in the adhesive layer for a given applied load were deduced using a continuum mechanics approach based upon a shear-lag analysis.[9] In this, only longitudinal tensile deformations in the adherends and shear deformations in the adhesive layers are included. The adherends are treated as linear elastic materials, but bonded with an

elastic-perfectly plastic adhesive having a shear stress/strain curve defined by the various parameters illustrated in Figure 3. From consideration of compatibility and equilibrium for the simplified system of deformations in the joint, differential equations are set up which are solved computationally using a piecewise discretisation of the overlap length. Because only shear deformations in the adhesive are considered, the resulting shear stress distribution consists of an elastic region at the centre of the overlap and, for sufficiently large applied loads, regions of uniform stress at the edges of the overlap, where plastic deformation has occurred. This is illustrated in the shear stress distribution shown in Figure 1. Although after yielding in the adhesive layer the shear stress becomes uniform, the shear strain does not and is a maximum at the edges, whether or not yielding has occurred.

The various mechanical properties shown schematically in Figure 3, which were required for the analysis of the shear stress in the adhesive, were measured experimentally, as discussed later.

Since, as expected, the CFRP/steel double-lap joints were experimentally found *not* to fail by shear failure of the adhesive, the shear-lag analysis was carried out only as a basis for establishing the dimensions of the basic joint geometry.

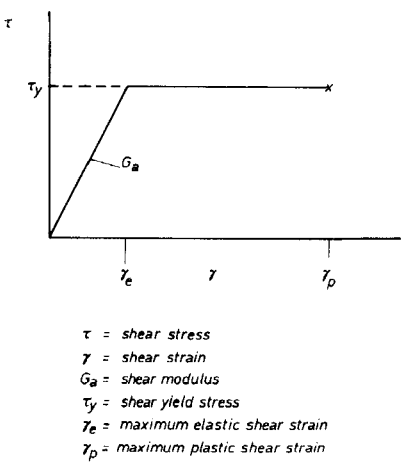

FIGURE 3 Schematic diagram of elastic-plastic behaviour of adhesive.

Tensile stresses The distribution of tensile stress, due to the direct stresses acting normal to the adhesive layer, in the adhesive and inner (CFRP) adherend was determined using a finite element analysis. This method of analysis was selected because, as expected, tensile cracking in the adhesive and/or interlaminar failure of the inner CFRP adherend at the end of the overlap were the primary cause of joint failure, and limited the joint strength that could be attained. The finite element technique (FET) enables such localised phenomena to be readily considered. For example, the effects of tapering the outer steel adherends, increasing the adhesive thickness and changing the shape of adhesive fillet may be readily described.[10,11]

The programs that have been used were developed specifically for the analysis of adhesive joints, so that both geometrical non-linearities (large displacements) as well as non-linear material behaviour may be accounted for. An automated mesh generation scheme was also used to enable changes in joint geometry to be made relatively easily.

The analysis was carried out in two dimensions, a state of plane strain across the width of the joint being assumed throughout. In the model, both the steel and CFRP adherends were represented as linearly elastic materials. However, so that joint failure based on a cohesive failure of the adhesive could be predicted, it was necessary to model the adhesive as an elastic-plastic material. To represent the yield behaviour of the adhesive, a yield criterion was used which is a function of both the hydrostatic as well as the deviatoric stress component, and is of the form[12]

$$[J_1(S-1) + (J_1^2(S-1)^2 + 12J_2S)^{1/2}]/2S = Y_T \qquad (1)$$

J_1 and J_2 are the first and second stress invariants where, for stress components $(\sigma_x, \sigma_y, \sigma_z, \tau_{xy}, \tau_{xz}, \tau_{yz})$,

$$J_1 = \sigma_x + \sigma_y + \sigma_z,$$
$$J_2 = \tfrac{1}{2}(\bar{\sigma}_x^2 + \bar{\sigma}_y^2 + \bar{\sigma}_z^2) + \tau_{xy}^2 + \tau_{xz}^2 + \tau_{yz}^2,$$
$$\sigma_x = \bar{\sigma}_x - J_1/3 \quad \text{etc},$$

and

$$S = Y_c/Y_T$$

where Y_c and Y_T are the yield stresses in uniaxial compression and tension respectively.

The value of Y_T thus represents the degree of hardening that has taken place after yielding and is determined from an equivalence of plastic work based on the uniaxial tensile properties of the adhesive.

In the application of the FET to adhesive joints it has been found that singularities arise at corner points in the geometry which, in the model, are perfectly sharp and are also on the boundary between the adherend and adhesive materials. In order to overcome the difficulties associated with these points, it has been found that the introduction of a small degree of local rounding into the finite element model in the critical regions, provides a more reliable basis for the prediction of joint strength.[13] Details of the modifications used here are given in the Appendix.

Failure criteria In selecting suitable failure criteria, it is first necessary to consider the various modes of failure which are likely. Possible failure modes include:

i) Adhesion failure at the CFRP/adhesive or steel/adhesive interface.

ii) Shear failure of the adhesive.

iii) Tensile cracking in the adhesive layer.

iv) Transverse or translaminar (tensile) failure of the CFRP.

v) Tensile fracture of the CFRP or steel adherends away from the overlap.

Assuming even a minimum surface pre-treatment procedure has been used for the adherends prior to joint preparation and no environmental attack on the bonded joint has occurred, then type (i) is unlikely. Obviously type (v) failure would represent the maximum joint strength that could be obtained, with a joint design efficiency of 100%. Failure types (ii), (iii) and (iv), therefore, need to be considered.

For type (ii) failure, a failure criterion based upon the maximum plastic strain, γ_p, that the adhesive can withstand in shear has been employed for the shear-lag analysis. For types (iii) and (iv) a limiting maximum principal tensile strain in the adhesive and limiting transverse tensile stress in the CFRP have been employed for the finite element analysis.

EXPERIMENTAL

Materials

The adhesive was a commercially available rubber-toughened epoxy resin cured by an accelerated dicyandiamide hardener. The curing schedule employed was two hours at 120°C.

The adherends were high-tensile steel (2 mm in thickness) and a unidirectional CFRP composite (3 mm in thickness), based upon an epoxy matrix.

Material characterisation

The tensile stress-strain properties of the adhesive were measured by testing bulk specimens which had been cast and machined into cylindrical "hour-glass" shaped test pieces. The parallel gauge length of each of these specimens was carefully polished, in order to avoid premature failure due to surface scratches, before being deformed at a constant strain rate of $0.05\,min^{-1}$ in a screw-driven test machine. A typical true stress versus strain curve is shown in Figure 4.

The shear properties of the adhesive were determined in pure

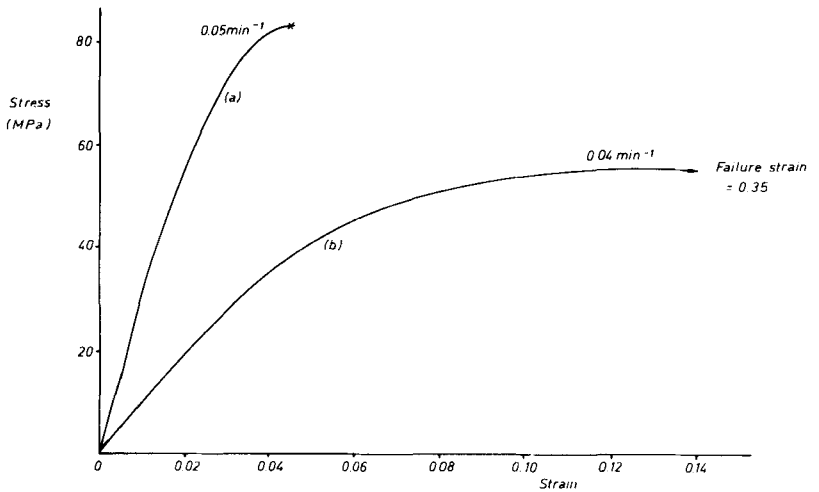

FIGURE 4 Stress versus strain curves for the rubber-modified epoxy adhesive. (a) Uniaxial tension (b) Pure shear.

shear by loading bulk cylindrical specimens of the adhesive in torsion at a constant rate of twist, of $0.04\,min^{-1}$. From the measured torque *versus* twist curve, a shear stress–strain curve was derived using the correction due to Nadai.[14] A typical pure shear stress *versus* strain curve is also shown in Figure 4, and the relationship between the tensile and shear curves is as previously reported[4] for epoxy polymers.

It should be noted that, although the normal cure condition for the adhesive was 120°C for 2 h, in the manufacture of bulk specimens of the adhesive, the cure temperature was reduced to 90°C and the time increased to 12 h. This was necessary to avoid excessive heat build-up in the material from the exothermic cure reaction. However, cylindrical butt joints were also produced with thin glue lines (0.5–1.5 mm) under the normal cure conditions and the shear stress–strain response measured from a torsion test. At equivalent rates of straining, the shear modulus and maximum shear

TABLE I
Material properties used in theoretical stress analyses and failure predictions

(a)	Adhesive (elastic-plastic)	
	Young's modulus, E_a,	3.05 GPa
	Tensile fracture stress, σ_{af},	82 MPa
	Tensile fracture strain, ε_{af},	0.0475
	Shear modulus, G_a,	1.13 GPa
	Shear yield stress, τ_Y,	54 MPa
	Max. elastic shear strain, γ_e,	0.055
	Max. plastic shear strain, γ_p,	0.35
	Poisson's ratio, ν_a,	0.35
	S [constant in Eqn. (1)]	1.24
(b)	High-tensile steel adherend (elastic)	
	Young's modulus, E_s,	210 GPa
	Poisson's ratio, ν_s,	0.29
(c)	Unidirectional CFRP (elastic)	
	Longitudinal tensile modulus, E_{cl},	140 GPa
	Transverse tensile modulus, E_{ct},	7 GPa
	Interlaminar shear modulus, G_c,	4.5 GPa
	Longitudinal and transverse Poisson's ratio, ν_c,	0.3
	Interlaminar, transverse strength	40 ± 6 MPa
	Longitudinal tensile strength	1400 MPa

stress obtained from the butt joint tests agreed to within 3 per cent of those derived from the measurements on the bulk specimens. The physical properties of the high-tensile steel and CFRP adherends were taken from the manufacturers' literature. The values for the various parameters needed for the theoretical analysis of the stress distributions in the joints are given in Table I. For the finite element analysis, the yield behaviour of the adhesive was based on the uniaxial tensile stress–strain curve in Figure 4.

Joint preparation and testing

The outer high-tensile steel adherends were $200 \times 15 \times 2$ mm and the inner CFRP adherend was $200 \times 15 \times 3$ mm. The surface of the high-tensile steel adherend which was to be bonded was first subjected to a liquid and vapour degreasing bath of 1,1,1 trichloroethane, grit-blasted with 180–220 mesh alumina, degreased again, then finally allowed to air dry. The surface of the CFRP adherend was first subjected to a solvent clean by wiping with a 1,1,1 trichloroethane soaked cotton-rag, lightly abraded, solvent wiped again, and then allowed to air dry. The adherends were placed in a silicone rubber mould and the joint formed by pouring adhesive, pre-warmed to about 60°C to reduce its viscosity, in the empty spaces in the mould. The silicone rubber moulds were cast around formers, shaped to give the required joint design, with the required overlap-length, type of adhesive fillet, and so on. The thickness of the adhesive layer employed was 1 mm. The adhesive was cured by placing the mould in an oven and heating at 120°C for 2 h. To test the adhesive joints, end tabs were bonded to the CFRP central adherend and the joint was loaded at a constant displacement rate until fracture occurred.

RESULTS AND DISCUSSIONS

Theoretical analyses

Shear stresses The results of the shear-lag analysis, treating the adherends as elastic materials and the adhesive as an elastic-plastic material, are shown in Figure 5. The two design variables are the thickness of adhesive layer, t_a, and the overlap-length, L. The

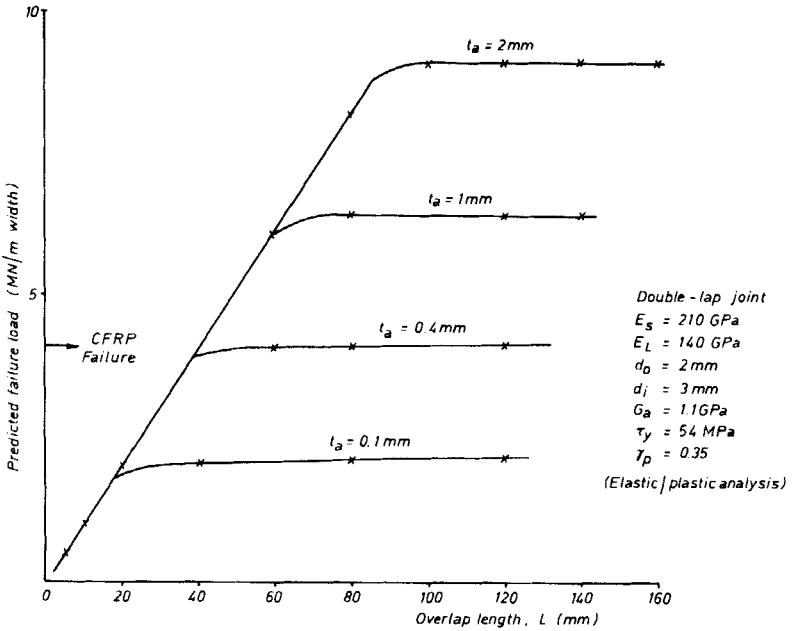

FIGURE 5 Predicted failure load per unit width of joint versus overlap-length for simple double-lap joint calculated from analysis of shear-stress concentrations in joint. (d_o and d_i are the thicknesses of the outer and inner adherends respectively).

predicted failure load for the basic double-lap joint (Figure 2, Design 1) shown as a function of the overlap length, L, and the relationship for a given t_a value shows the well-established[15] initial linear increase in failure load followed by a plateau as the value of L increases. Also indicated in Figure 5 is the failure load at which tensile fracture of the CFRP, the weaker of the adherends, occurs. Obviously, if the joint failed at this load it would be 100% efficient, where the joint efficiency is defined as the strength of the joint divided by the tensile strength of the weaker adherend. The analysis of shear stresses, therefore, suggests that for an adhesive thickness, t_a, of 1.0 mm then an overlap-length, L of 60 mm or more should ensure a 100% efficient joint. However, as discussed later, shear failure of the adhesive was not the observed failure mode, but interlaminar failure of the CFRP at the end of the overlap-length occurred at a failure load of approximately 1 MN/m width.

Nevertheless, the analysis shown in Figure 5 does suggest that a plateau strength level is achieved at values of L of about 60 to 80 mm and, therefore, an overlap length of 80 mm was adopted for future computations of the peeling stresses and the experimental studies.

Tensile stresses The finite element analysis was conducted to determine the effect of the tensile stresses normal to the loading direction (Figure 1), both in the CFRP inner adherend and in the adhesive layer. Further, the various joint designs in Figure 2 were considered in order to reduce the magnitude of such stresses.

Considering firstly the distribution of tensile stresses in the CFRP, then, for all of the joint designs investigated, the maximum transverse stresses σ_{tm} in the CFRP occurred in the region adjacent to the edges of the outer steel adherends as expected from Figure 1. The values of σ_{tm} for each joint when subject to a load of 1 MN/m width derived from the finite element results with elastic adhesive properties, are given in Table II. Comparing the values for designs 1–3 (Figure 2), it would appear that tapering the outer adherends has an insignificant effect on reducing σ_{tm} in the CFRP. In Figure 6, a contour plot based on an interpolation of the Gauss point values

TABLE II
Predictions of the maximum transverse stresses, σ_{tm}, in the CFRP inner adherend from elastic finite element analysis

Design No. (See Figure 2)	Description	Fillet angle	σ_{tm} in CFRP[a] (MPa)
1	Basic	~90°	38
2	Outside taper	~90°	37
3	Inside taper	~90°	36.5
4	Adhesive fillet	45°	16
4	Adhesive fillet	30°	10
4	Adhesive fillet	17°	10
5	Inside taper + Adhesive fillet	45°	13
5	Inside taper + Adhesive fillet	30°	6.5
5	Inside taper + Adhesive fillet	17°	5

[a] Applied load on joint = 1 MN/m.

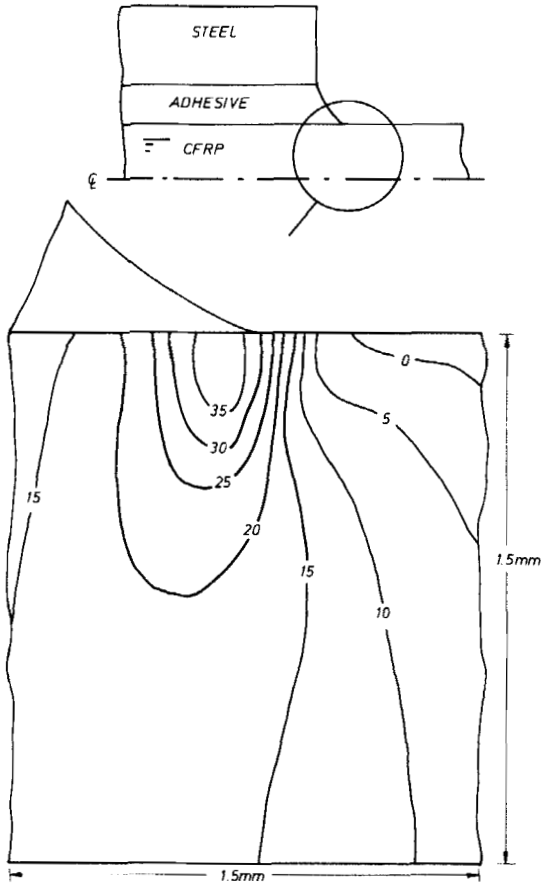

FIGURE 6 Joint Design 1: Transverse stresses (MPa) in the CFRP, for an applied joint load of 1 MN/m.

of the transverse stresses is shown in the critical region of design 1. For this case, as with designs 2 and 3, there is a large stress concentration adjacent to the very edge of the adhesive layer. Because of the abrupt edge to the adhesive layer, the transfer of the load from inner CFRP adherend to the outer steel adherends is focussed in this local edge region; the transverse stresses in the CFRP decay rapidly away from the edge region towards the

centre-line of the joint and longitudinally away from the overlap. This pattern of load transfer and concentration of stress is affected only slightly by including either the outside or inside taper of designs 2 and 3. It is worth noting that prediction of the magnitude of the concentration of transverse stress would be very difficult by closed form analytical methods, so that resorting to the use of finite elements appears justifiable.

The introduction of an adhesive fillet as in design 4 does lead to an appreciable reduction in the maximum transverse stress in the CFRP. The relatively small modification of a 45° fillet results in a reduction in the stress concentration by almost a factor of two. The action of the fillet is to provide less of a focus for the transfer of load at the edge of the overlap resulting in a more even distribution of transverse stress. Further advantage can be gained by reducing the fillet angle to 30°. The distribution of transverse stress in the CFRP for this case is shown in Figure 7. Compared with the distribution for design 1 in Figure 6, the stress concentration at the corner has clearly been avoided and there is little variation in stress through the thickness of the CFRP. Reducing the fillet angle further results in no further reduction in stress concentration. For this design, with a fillet angle of less than about 35°, the maximum transverse stress in the CFRP is reduced to almost one third of that of the basic design. The position at which the maximum stress occurs also depends on the angle of the fillet. For angles greater than 35°, the maximum value occurs in the CFRP at the outer surface, adjacent to the edge of the adhesive layer, as indicated in Figure 2 as point A in design 4. For angles less than 35°, the maximum value occurs at point B in Figure 2, at the interface, but within the adhesive fillet, approximately 0.5 mm outside the overlap. The relative magnitude of the stresses at the two points will depend on the relative stiffness of the paths by which load is transferred from inner to outer adherends, *i.e.*, the transverse stiffness of the paths through points A and B. The former depends on the angle of the fillet and becomes less as the fillet angle is reduced. The latter is relatively insensitive to the fillet angle, so that when the fillet angle becomes less than 35°, the value and location of the maximum stress varies little with the angle.

In design 5, the combination of the internally tapered steel adherend with an adhesive fillet results in further reductions in the

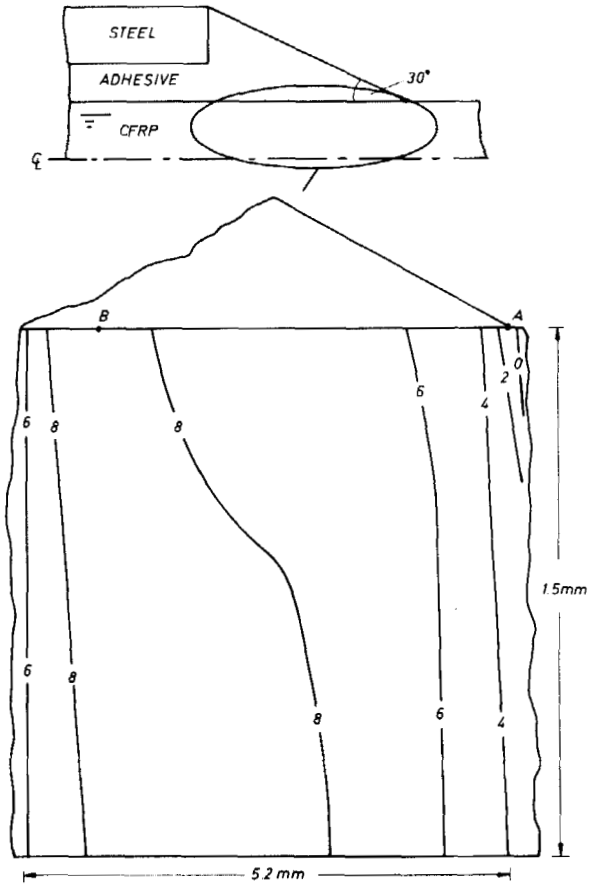

FIGURE 7 Joint Design 4 ($\alpha = 30°$): Transverse stresses (MPa) in the CFRP, for an applied joint load of 1 MN/m.

transverse stress concentration in the CFRP. Again, this is achieved because the transverse stiffness at the edge of the overlap is reduced and, with an adhesive fillet present, the effect of the taper is significant. For design 5, as with design 4, the maximum occurs at the edge of the fillet for small fillets, *i.e.*, at point A in Figure 2. For larger fillets with angles of 45° or less, such as the 30° case shown in Figure 8, the maximum transverse stress occurs inside the adhesive

fillet at point B. With larger fillets, point B moves further away from the edge of the overlap, *i.e.*, from 1.7 to 2.0 to 2.7 mm for fillet angles corresponding to 45°, 30° and 17° respectively. Little further benefit would appear to be gained by increasing the size of the fillet so that the angle is less than 17°.

Turning to the analysis of transverse tensile stresses in the adhesive layer, then the results of the finite element analyses also

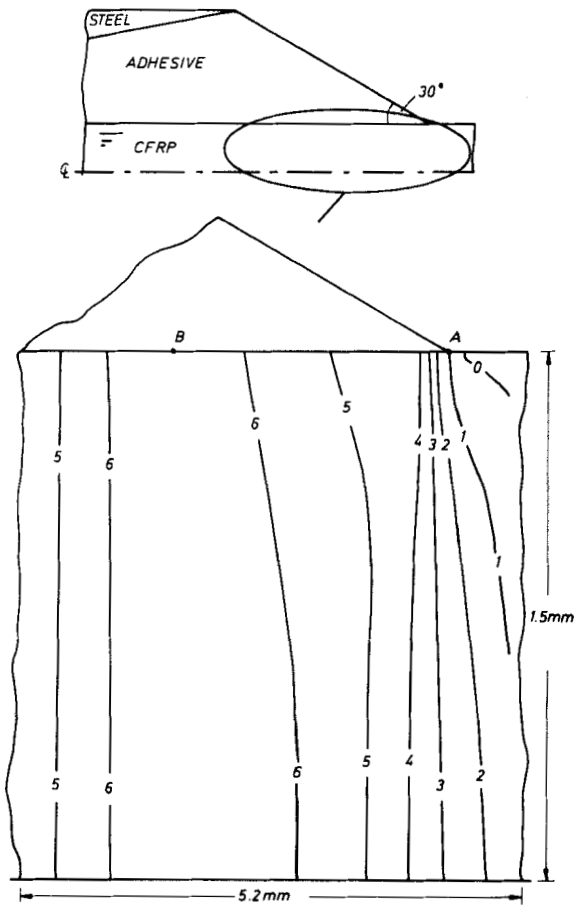

FIGURE 8 Joint Design 5 ($\alpha = 30°$): Transverse stresses (MPa) in the CFRP, for an applied joint load of 1 MN/m.

give the values of the stress components at various locations in the adhesive. From these, the direction and magnitude of the principal stresses are derived. When joint failure is initiated by a cohesive failure of the adhesive, it has been found for elastic adhesive properties that failure initiates in regions of maximum stress concentration in the adhesive, and cracks propagate at right angles to the direction of the maximum principal stresses. For elastic-plastic adhesive properties, the strains are also important. However, for the joints examined here, the location and direction of the maximum stresses given from the elastic analyses are coincident with the location and direction of the critical conditions given from the elastic-plastic analyses. Thus, by examination here of the principal stress distributions from the elastic analyses, the locations and directions of cohesive failure in the adhesive may be predicted. However, as will be considered later, in order to predict joint strength, the adhesive strains from the elastic-plastic analyses must be determined.

Principal stress plots are shown in Figures 9, 10 and 11, corresponding to a square-edged adhesive layer (Design 1), a 30°

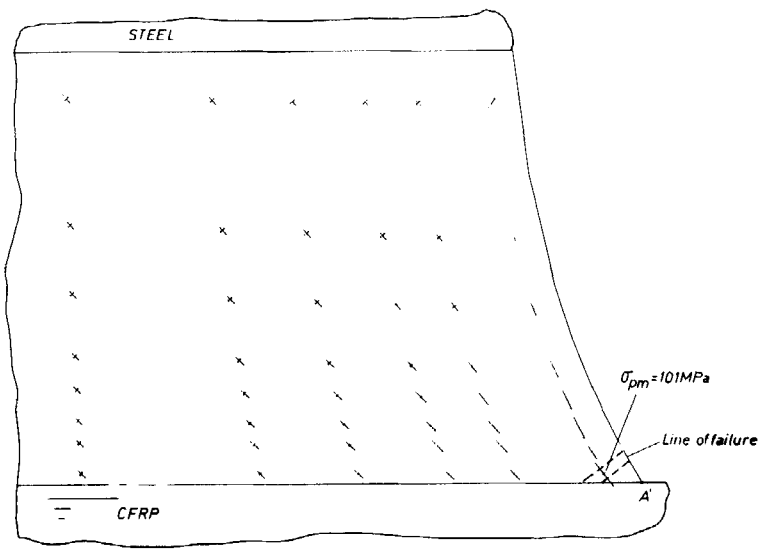

FIGURE 9 Joint Design 1: Principal stress distribution, σ_p, in the adhesive at the edge of the overlap, for an applied joint load of 1 MN/m.

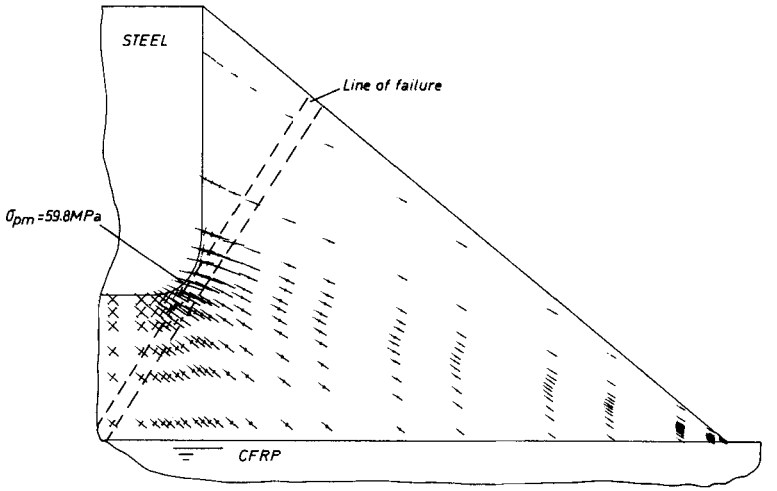

FIGURE 10 Joint Design 4 ($\alpha = 30°$): Principal stress distribution, σ_p, in the adhesive at the end of the overlap, for an applied joint load of 1 MN/m.

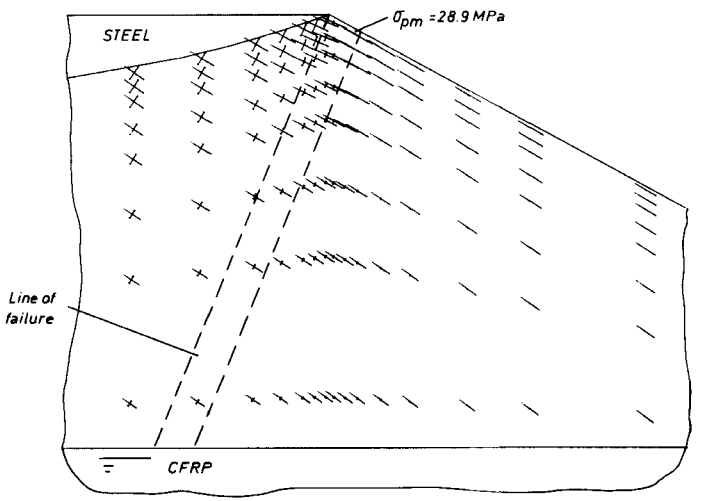

FIGURE 11 Joint Design 5 ($\alpha = 30°$): Principal stress distribution σ_p, in the adhesive at the end of the overlap, for an applied load of 1 MN/m.

fillet (Design 4) and a 30° fillet with an internally tapered outer adherend (Design 5). In each case, the results are shown for a 1 MN/m width applied load with the adhesive modelled as a linearly elastic material.

For the adhesive layer of design 1 in Figure 9, the maximum stress occurs close to the interface with the central CFRP adherend and any crack initiating in this region will be driven towards the interface. With an adhesive fillet, as in Figure 10, failure is expected to initiate in the vicinity of the corner of the outer steel adherend and a crack will propagate through the fillet and again down to the interface with the CFRP. Thereafter, either an adhesive failure at the interface or a transverse failure of the CFRP will occur. With the tapered joint in Figure 10, removing the corner of the steel adherend leads to a relieving of the stress concentration at the corner and now the maximum occurs at the outer surface of the adhesive fillet close to the outer steel adherend corner. Again, cracks initiated in this region would be expected to propagate through the fillet to the interface with the CFRP as indicated.

The relative values of the largest principal stresses in the adhesive predicted for each of the joints discussed are an indication of the relative strengths that might be expected if cohesive failure in the adhesive were to take place throughout. However, to predict joint strength based on this mode of failure, the elastic-plastic adhesive properties must be included in the model. With yielding and plastic flow in the critical regions of the joint, the stresses become more evenly distributed, so that the distributions discussed do not strictly apply for failure.

Comparison between experiment and theory

The experimentally determined failure loads for the various joint designs are shown in Table III. In all cases, the mode of failure was *not* by shear failure of the adhesive, but by apparent interlaminar fracture of the CFRP inner adherend. This interlaminar fracture occurred in the region of the overlap where the steel outer adherends terminated. This failure mode is obviously caused by the transverse tensile stresses in the joint, as described earlier and shown in Figure 1. However, there are two possible failure mechanisms which may account for the above observations. Either

excessive transverse tensile stresses at the edge of the joint close to the interface results in interlaminar failure of the CFRP, or concentrations of the principal stresses in the adhesive result in yielding and straining to failure under predominantly tensile forces. Since the latter will result in cracks running through the adhesive to the interface, so that thereafter interlaminar failure of the CFRP may occur, it may not be clear in the first instance which mechanism is responsible for failure from the fractured surfaces of the joint.

By applying suitable failure criteria to the finite element results, it is possible to predict the load required for failure to occur by each mechanism. For interlaminar failure of the composite, a maximum tensile transverse stress of 40 ± 6 MPa has been found experimentally.[5] For the cohesive failure of the adhesive, a maximum principal tensile strain criterion has been found to predict joint strength reasonably.[11] The criterion is applied to the point in the adhesive at which the maximum principal tensile stress is greatest. Under this condition, the adhesive will show the least ductility before fracture, as is the case for the failure of the adhesive in bulk in Figure 4. Here, the limiting value of 0.0475 has been used equal to the strain at failure in bulk uniaxial tension, which closely resembles the state of stress in the critical regions of the adhesive.

The predicted joint strengths are compared with the experimental values in Table III. For design 1, which has no adhesive fillet, interlaminar CFRP failure is predicted to occur before failure in the adhesive. The elastic analyses indicated that tapering in designs 2 and 3 would have little effect on the predicted strength based on cohesive failure of the adhesive for design 1, so that CFRP failure is expected for these designs also. Therefore, the CFRP failure predictions for designs 1–3 are based on the results of the elastic analysis. This is justifiable because the results of the elastic-plastic analysis for design 1 indicated that yielding of the adhesive has an insignificant effect on the magnitudes of the transverse CFRP stresses predicted. Thus, based on the CFRP transverse failure mode, the strengths of each of the joints, designs 1–3, are expected to be similar. These predictions are in keeping with the experimental evidence that tapering of the adherend alone has little influence on the joint strength. The predicted strengths are all somewhat higher than the experimental values, although the discrepancies are small.

TABLE III
Comparison of experimental joint strengths with theoretical predictions

Joint design No.	Description	Fillet angle	Observed failure load (MN/m)	Theoretical prediction: Interlaminar CFRP failure[a] (MN/m)	Theoretical prediction: Tensile adhesive failure[b] (MN/m)
1	Basic	90°	0.93	1.05[c]	1.6
2	Outside taper	90°	0.89	1.08[c]	—
3	Inside taper	90°	0.94	1.10[c]	—
4	Adhesive fillet	45	—	2.7[c]	—
4	Adhesive fllet	30	—	4.24[c]	2.0
4	Adhesive fillet	17	—	4.24[c]	—
5	Inside taper + Adhesive fillet	45	2.72	3.53	4.0
5	Inside taper + Adhesive fillet	30	3.05	7.44	3.3
5	Inside taper + Adhesive fillet	17	2.80	9.08	2.4

[a] Based upon a maximum transverse, interlaminar strength of 40 MPa.
[b] Based upon a maximum principal (tensile) strain of 0.0475.
[c] From elastic analysis (otherwise elastic-plastic analysis).

For the filleted joint, as in design 4, the results from the elastic analysis indicated that the failure load based on initial tensile failure in the adhesive, as well as that based on interlaminar CFRP failure, increases as the fillet size increases. For the 30° fillet angle case, the elastic-plastic analysis predicts that the latter is always greater. Thus, failure is expected always to initiate in the adhesive for this design. Once a crack has formed, as in Figure 10, the geometry of the joint becomes effectively that of design 1 and, since the failure load for that joint has already been exceeded, the interlaminar failure of the CFRP follows instantaneously. Since design 4 did not appear to offer such major improvements in failure load compared to design 5 (see below), experiments were not conducted on design 4.

For the joints combining the taper and fillet, as in design 5, increasing the size of the fillet is predicted to increase joint strength based on CFRP interlaminar failure and to decrease joint strength based on initial failure in the adhesive. Thus, it is predicted that there is a fillet angle between 30° and 45° above which interlaminar

CFRP fracture is responsible for joint failure and below which adhesive tensile fracture is responsible. Again, for the 45° fillet case, the predicted strength based on CFRP failure is somewhat high, so that, just as for designs 1–3, a lower value for the transverse strength would give a better prediction. It is, therefore, possible that the transverse strength used (from ref. 5) was too high.

As the fillet size is increased so that the fillet angle becomes less than 30°, the joint strength is reduced as tensile failure in the adhesive occurs at lower loads. This is because the stress concentration in the critical region indicated in Figure 11 increases, as more load is transferred through the fillet to this point. Again, once a crack has propagated through the adhesive, the joint becomes similar to design 3 and transverse failure of the CFRP follows.

CONCLUSIONS

It has been found experimentally that, by modifying the geometry of the double lap joint in the critical regions at the edge of the overlap, significant increases in the strength of the joint may be achieved. In particular, by a combination of adherend tapering and including a fillet of adhesive at the edge of the overlap, a 3-fold increase in joint strength is obtained, giving a joint efficiency of approximately 73%. By modelling the joint using finite elements, it has been demonstrated that this increase in strength is achieved because the concentration in transverse tensile stress in the CFRP is reduced. Premature interlaminar failure in the CFRP is thus avoided and in the modified joint failure now initiates in the adhesive. Therefore, in principle, the observed increase in joint strength may have been predicted from the finite element analysis of the joint geometries, requiring only a knowledge of the material properties of the component parts.

References

1. O. Volkersen, *Luftfahrforsch* **15,** 41 (1938).
2. L. J. Hart-Smith, *Developments in Adhesives—2,* A. J. Kinloch, Ed. (Appl. Sci. Pub., London, 1981), p. 1.
3. O. Volkersen, *Construction Metallique* **4,** 3 (1965).

4. A. J. Kinloch and R. J. Young, *Fracture Behaviour of Polymers*, (Appl. Sci. Pub., London, 1983).
5. P. D. Ewins, *Tensile and Compressive Test Specimens for Unidirectional CFRP*, TR 71217, (Royal Aircraft Establishment, Farnborough, 1971).
6. J. B. Cushman, S. F. McCleskey and S. H. Ward, *Design, Fabrication and Test of Graphite/Polyimide Composite Joints and Attachments*, CR 3601 (National Aeronautics and Space Administration Washington DC, 1983).
7. A. D. Crocombe and R. D. Adams, *J. Adhesion* **13,** 141 (1981).
8. F. Thamm, *J. Adhesion* **8,** 301 (1975).
9. Engineering Services Data Unit (UK) Reoprt, *Inelastic Shear Stresses and Strains in the Adhesives Bonding Lap Joints Loaded in Tension or Shear*, No 79016, (London, 1979).
10. R. D. Adams and N. A. Peppiatt, *Adhesion—2*, K. W. Allen, Ed. (Appl. Sci. Pub., London, 1978) p. 105.
11. J. A. Harris and R. D. Adams, *Int. J. Adhesion, Adhesives*, **4,** 65 (1984).
12. R. Raghava, R. M. Caddell and G. S. Y. Yeh, *J. Materials Sci.*, **8,** 225 (1973).
13. J. A. Harris and R. D. Adams, To be published.
14. A. Nadai, *Plasticity: A Mechanics of the plastic state of matter*, (McGraw Hill, New York, 1931), p. 128.
15. A. J. Kinloch, *J. Materials Sci.*, **17,** 617 (1982).

Appendix

Modification to the finite element model at critical points in the various joint geometries was achieved by locally rounding the associated corners in the finite element grid. The critical points for designs 1–3 are designated as '*A*' in Figure 2, while for designs 4 and 5 they are designated as '*C*' and '*D*' respectively. Basically, the rounding was achieved by transforming the finite element grid locally to give boundaries that are parabolic in nature. These modifications for each joint analysed are illustrated in Figure A1.

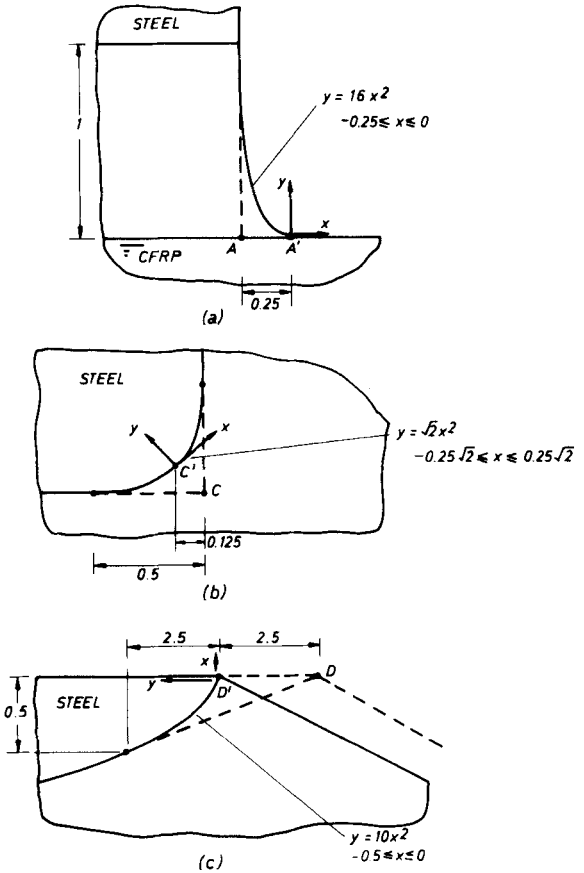

FIGURE A1 Details of geometry modifications for the finite element models: (a) Designs 1–3, (b) Design 4, (c) Design 5. Dimensions in mm.